

## JOURNAL OF LIMNOLOGY

DOI: 10.4081/jlimnol.2023.2144

## SUPPLEMENTARY MATERIAL

### Multidecadal analysis of Lake Garda water balance

Luigi Hinegk,<sup>1</sup> Luca Adami,<sup>1\*</sup> Sebastiano Piccolroaz,<sup>1</sup> Marina Amadori,<sup>1,2</sup>  
Marcello Moretti,<sup>3</sup> Marco Tubino,<sup>1</sup> Marco Toffolon<sup>1</sup>

<sup>1</sup>Department of Civil, Environmental and Mechanical Engineering  
Department (DICAM), University of Trento, Via Mesiano 77, 28122  
Trento

<sup>2</sup>Institute for Electromagnetic Sensing of the Environment, National  
Research Council, Via Corti 12, 20133, Milan

<sup>3</sup>Interregional Agency for the Po River (AIPo), Vicolo Canove 26, Mantova,  
Italy

\*Corresponding author: [luca.adami@unitn.it](mailto:luca.adami@unitn.it)

## Water balance components

In this section, we briefly review all the formulas used in this work, with a specific focus on the open-surface lake evaporation  $EV_L$  and catchment reference evapotranspiration  $ET_0$ . In particular, the final formulation will be always expressed in the same units ( $mm\ day^{-1}$ ) and in accordance with the units reported in the list of symbols, except where otherwise specified in the Method's description.

## Open-surface lake evaporation

Penman (1948) proposed a combined aerodynamic-energy equation, avoiding the need for lake surface water temperature data, for the open-surface lake evaporation is:

$$EV_L^{Pen} = \frac{\Delta}{\Delta + \gamma} \frac{R_{nw}}{\lambda} + \frac{\gamma}{\Delta + \gamma} f(u)(e_s - e_a), \quad (S.1)$$

where  $R_{nw}$  is the net daily radiation at the water surface, evaluated using a proper albedo for open-water ( $\alpha_l = 0.08$ ). On the basis of the discussion reported in Section S4 in McMahon *et al.* (2013), we considered the Penman's 1956 wind function:

$$f(u) = 1.313 + 1.381u_2, \quad (S.2)$$

where  $u_2$  is the wind velocity at 2 m above the lake surface.

Jensen and Haise (1963) developed an empirical relationship to estimate evaporation starting from air temperature and incoming solar radiation data as follows:

$$EV_L^{JH} = 0.03523R_s(0.014T_a - 0.37), \quad (S.3)$$

where  $R_s$  is the incoming solar radiation ( $Wm^2$ ),  $T_a$  is the air temperature and 0.03523 is the coefficient of conversion from  $Wm^2$  to  $mm\ day^{-1}$ . Due to its simplicity and reliability, eq. (S.3) was found a low-cost method to estimate evaporation by Majidi *et al.* (2015).

Starting from the equation proposed by Penman (1948), Priestley and Taylor (1972) provided an alternative estimation of over-lake evaporation that excludes the aerodynamic component:

$$EV_L^{PT} = \alpha_{PT} \left( \frac{\Delta}{\Delta + \gamma} \frac{R_{nw}}{\lambda} - \frac{G}{\lambda} \right), \quad (S.4)$$

where  $\alpha_{PT} = 1.26$  is the Priestley-Taylor constant for open-surface water and  $G$  is the heat flux term ( $MJm^{-2}day^{-1}$ ).

In case of missing wind data, Valiantzas (2006) developed an alternative method to estimate evaporation by simplifying the original Penman equation as follows:

$$EV_L^{Val} = 0.047R_s(T_a + 9.5)^{0.5} - 2.4\left(\frac{R_s}{R_a}\right)^2 + 0.06(T_a + 20)\left(1 - \frac{\phi_{mean}}{100}\right), \quad (S.5)$$

where  $\phi_{mean}$  is the mean daily relative humidity.

The Dalton-type or mass transfer method estimates the open-surface lake evaporation on the basis of the original formulation proposed by Dalton in 1802:

$$EV_L^{Dal} = C_{emp}f(u)(e_s - e_a), \quad (S.6)$$

where  $C_{emp}$  is an empirical constant,  $f(u)$  is a wind function,  $e_s$  is the saturation vapour pressure at the evaporating surface ( $hPa$ ) and  $e_a$  the atmospheric vapour pressure ( $hPa$ ).

In this study, we considered the formulation reported in Fink *et al.* (2014), eq. 11-13 calibrated for Lake Zürich and additionally applied to Lake Constance. Such formulation has already been used for producing satellite-based lake evaporation maps for Lake Garda by Matta *et al.* (2022). In particular, the formulation of Fink *et al.* (2014) gathers  $C_{emp}$  and  $f(u)$  in a sole empirical function named  $f$  (expressed in  $Wm^{-2}mbar^{-1}$ ) that includes not only the wind velocity ( $u_{10}$ , in  $ms^{-1}$  and evaluated at 10 m above the lake surface), but also air and water temperature. Such empirical function is estimated according to the Magnus approximation as follows:

$$f = 4.8 + 1.98u_{10} + 0.28(T_w - T_a). \quad (S.7)$$

The saturation vapour pressure at the evaporating surface  $e_s$  is defined as follows:

$$e_s = 0.611exp\left(\frac{17.62T_w}{T_w + 243.12}\right). \quad (S.8)$$

As the Fink *et al.* (2014) formulation expresses  $EV_L^{Dal}$  in  $Wm^{-2}$ , the coefficient of conversion 0.03523 was applied to eventually obtain the values in  $mm\ day^{-1}$ .

### Lake surface water temperature.

In this application, we estimated the LSWT of Lake Garda starting from local estimates of AT by implementing the air2water model (Toffolon *et al.*, 2014; Piccolroaz, 2016; Piccolroaz *et al.*, 2018). In particular, we rely on the results of Piccolroaz *et al.* (2020), who adopted the value of air temperature from the global atmospheric reanalysis ERA-20C European Centre for Medium-Range Weather Forecasts, 2014 for Lake Garda as an input, and the data provided by the satellite-derived LSWT observations (ARC-Lake v3) as the target. The root mean square error was 0.79C, with a Nash-Sutcliffe Efficiency (NSE) of 0.98. Following the same procedure, since the reanalysis ERA-20C provides air temperature data up to 2010, we extended the LSWT dataset up to 2020 through the reconstruction of the ERA-20C data on the basis of the available AT stations near Lake Garda.

### Catchment reference evapotranspiration

In this Section, we summarize the relations used for the estimation of the catchment reference evapotranspiration,  $ET_0$  ( $mm\ day^{-1}$ ), as reported in Allen *et al.* (1998) and McMahon *et al.* (2013). The final formulation will be expressed in accordance with the units reported in the list of symbols, except where otherwise specified in the method's description.

Hargreaves and Samani (1985) (hereafter HS) developed the following equation to estimate the reference crop evapotranspiration:

$$ET_0^{HS} = 0.0023R_a(T_{a,max} - T_{a,min})^{0.5} \left( \frac{T_{a,max} + T_{a,min}}{2} + 17.8 \right). \quad (S.9)$$

Ravazzani *et al.* (2012) proposed a modified version of the original HS equation for the Alpine region that includes the effect of the altitude of the recording station:

$$ET_0^{HSAlp} = (0.817 + 0.00022z)ET_0^{HS}, \quad (S.10)$$

where  $ET_0^{HS}$  is the original eq. (S.9), and  $z$  is the station elevation (m asl).

Starting from the original equation of Penman-Monteith, Allen *et al.* (1998) introduced the standardized reference crop evapotranspiration FAO56 Penman-Monteith equation:

$$ET_0^{FAO56PM} = \frac{0.408(R_n - G) + \gamma \frac{900}{T_{a,mean} + 273} u_2 (e_s - e_a)}{\Delta + \gamma(1 + 0.34u_2)}, \quad (S.11)$$

where  $R_n$  the net radiation at the crop surface ( $MJm^{-2}day^{-1}$ ),  $G$  the soil heat flux ( $MJm^{-2}day^{-1}$ ),  $T_{a,mean}$  the mean daily AT at 2 m height (C),  $u_2$  the wind speed at 2 m height ( $ms^{-1}$ ),  $e_s$  the saturation vapour pressure (kPa),  $e_a$  the actual vapour pressure (kPa),  $e_s - e_a$  the saturation vapour pressure deficit (kPa),  $\Delta$  the slope of saturation vapour pressure curve (kPa °C<sup>-1</sup>),  $\gamma$  the psychrometric constant (kPa °C<sup>-1</sup>).

The slope of saturation vapour pressure curve  $\Delta$  (kPa °C<sup>-1</sup>) at the air temperature  $T_a$  (C) can be estimated according to the following formula:

$$\Delta = \frac{4098 \left[ 0.618 \exp \frac{17.27T_a}{T_a + 237.3} \right]}{(T_a + 237.3)^2}. \quad (S.12)$$

The psychrometric constant  $\gamma$  (kPa °C<sup>-1</sup>) is as follows:

$$\gamma = 0.00163 \frac{P_{atm}}{\lambda}; \quad (S.13)$$

where  $\lambda$  is the latent heat of vaporization, which is  $2.45 MJm^{-2}day^{-1}$  (at 20 C), and  $P_{atm}$  (kPa) is the atmospheric pressure, which can be estimated as a function of the elevation  $z$  (m):

$$P_{atm} = 101.3 \left( \frac{293 - 0.0065z}{293} \right)^{5.26} \quad (S.14)$$

In case of data-missing contexts, Allen *et al.* (1998) proposed alternative procedures to estimate the net radiation, wind speed and humidity terms of eq. (S.11). In case of absence of air humidity data, the actual vapour pressure  $e_a$  (kPa) can be estimated as:

$$e_a = 0.611 \exp \left( \frac{17.27 T_{dew}}{T_{dew} + 237.3} \right), T_{dew} \approx T_{a,min}, \quad (S.15)$$

which assumes that the daily minimum air temperature  $T_{a,min}$  (C) can approximate the dew point temperature  $T_{dew}$  (C). Such assumption, and hence eq. (S.15), is valid for well watered cover crop locations, and further adjustment should be applied in case of arid region, humid and sub-humid climates.

In case of missing wind velocity data, Allen *et al.* (1998) recommend to use appropriate nearby weather stations or an average value of mean monthly wind speed at 2 m ( $u_2$ ) of  $2 \text{ ms}^{-1}$ , and, in any case, no less than  $0.5 \text{ ms}^{-1}$ .

### Radiation data

In case of no net radiation data recorded, appropriate estimates of solar radiation can be obtained as a function of latitude and the day of the year according to the work of Hamon *et al.* (1954). Here, we summarise such procedure as reported in Martin *et al.* (2018), to which interested readers are referred for further details. The extraterrestrial (solar) radiation,  $R_a$  ( $\text{Wm}^{-2}$ ), can be computed as follows (Martin *et al.*, 2018, Section III, eq. 11,12,13):

$$R_a = \frac{G_{sc}}{r^2} \left\{ \sin \left( \frac{\pi \theta}{180} \right) \sin(\delta) + \frac{12}{\pi} \cos \left( \frac{\pi \theta}{180} \right) \cos(\delta) [\sin(h_e) - \sin(h_b)] \right\} \Gamma, \quad (S.16)$$

$$r = 1.0 + 0.017 \cos \left[ \frac{2\pi}{365} (186 - D_y) \right], \quad (S.17)$$

$$\delta = \frac{23.45\pi}{180} \cos \left[ \frac{2\pi}{365} (172 - D_y) \right], \quad (S.18)$$

$$h_b = \frac{\pi}{12} [(h_r - 1) - \Delta t_s + a12] + b(2\pi), \quad (S.19)$$

$$h_e = \frac{\pi}{12} (h_r - \Delta t_s + a12) + b(2\pi), \quad (S.20)$$

$$\Delta t_s = \frac{E_a}{15} (L_{sm} - L_{lm}), \quad (S.21)$$

where  $G_{sc}$  is the solar constant ( $1390 \text{ Wm}^{-2}$ ),  $r$  is the relative Sun-Earth distance,  $\theta$  is the latitude (degrees),  $D_y$  is the day of the year (January 1 is  $D_y = 1$ ),  $\delta$  is the declination of the Sun,  $h_b$  is the hour angle (radians) at the beginning of the period over which the solar radiation at the edge of the atmosphere is being calculated,  $h_e$  is the hour angle (radians) at the ending of the period over which the solar radiation at the edge of the atmosphere is being calculated,  $h_r$  is the hour of the day (1-24),

$\Delta t_s$  is the fraction of an hour required to cross the sky between a standard meridian ( $L_{sm}$ , degrees) and the local meridian ( $L_{lm}$ , degrees),  $E_a$  is a coefficient related to the longitude ( $E_a = 1$  for west longitude,  $E_a = -1$  for east longitude),  $\Gamma$  is the correction factor for diurnal exposure to the radiation flux. The final values of  $R_a$  (from  $Wm^{-2}$  to  $MJm^{-2}day^{-1}$ ) was obtained applying the coefficient 0.0864.

The net shortwave solar radiation  $R_{ns}$  ( $Wm^{-2}$ ) is then evaluated as follows according to Allen *et al.* (1998):

$$R_{ns} = R_a(1 - R_s), \quad (S.22)$$

When missing values of  $R_s$  are not available, one can adopt the Hargreaves' radiation formula, which is based on air temperature differences as follows:

$$R_s = 0.16 \sqrt{T_{a,max} - T_{a,min}} R_a, \quad (S.23)$$

with 0.16 representing an adjustment coefficient for 'interior' locations (against 'coastal' locations). The net (longwave) radiation  $R_{nl}$  ( $Wm^{-2}$ ) can be derived from the following expression:

$$R_{nl} = \sigma \left[ \frac{T_{a,max,K}^4 + T_{a,min,K}^4}{2} \right] (0.34 - 0.14\sqrt{e_a}) \left( 1.35 \frac{R_s}{R_{so}} - 0.35 \right) \quad (S.24)$$

where  $\sigma$  is the Stefan-Boltzmann constant ( $4.9 \cdot 10^{-9} MJm^{-2}day^{-1}$ ),  $T_{a,max,K}$  is the maximum absolute temperature during the 24-hour period (K),  $T_{a,min,K}$  is the minimum absolute temperature during the 24-hour period (K),  $e_a$  is the actual vapour pressure (kPa),  $R_s/R_{so}$  is the ratio between the measured solar radiation ( $Wm^{-2}$ ) and the clear-sky radiation ( $Wm^{-2}$ ), namely the relative shortwave radiation. This term expresses the cloudiness of the atmosphere.

Thus, the net radiation  $R_n$  at the evaporative surface, which represents the input for the FAO-56 PM model (eq. (S.11)) is:

$$R_n = R_{ns} - R_{nl}. \quad (S.25)$$

Provincia Autonoma di Trento (2006) elaborated a coefficient of correlation between eq. (S.9) of Hargreaves and Samani (1985) and eq. S.11 of Allen *et al.* (1998) by adopting the available data of several meteorological stations of the Trentino Region and adopting a correction coefficient:

$$ET_0^{PGUAP} = 0.7ET_0^{HS}, \quad (S.26)$$

where  $ET_0^{HS}$  is the original Hargreaves-Samani equation, eq. (S.9).

Starting from the equations presented above and the land use data, we applied the crop coefficient  $K_c$  to obtain the potential evapotranspiration  $ET_p$  within the Sarca-Garda catchment as follows:

$$ET_p = ET_0 K_c, \quad (S.27)$$

where  $K_c$  is experimentally determined for each crop and varies according to the growth stage (Allen *et al.*, 1998). Since the  $K_c$  coefficient is calculated under standard crop conditions, i.e., well watered crop and optimal agronomic conditions, an additional factor  $\alpha$  is introduced to obtain the actual evapotranspiration  $ET_a = \alpha ET_p$ , thus considering the existence of water and environmental stresses (e.g., Mallucci *et al.*, 2019).

### Catchment and over-lake precipitation

The daily value of precipitation recorded from the available stations (Fig. S2) were spatialized according to the kriging approach (Goovaerts, 1997). The method was used to obtain spatially distributed maps of precipitation and air temperature (Fig. S4).

Fig.

### Surface outflow

The Mincio River represents the only outflow of Lake Garda, and its daily discharge is recorded since the XIX century near the lake headwaters. A first rating curve was constructed at the headwaters of Lake Garda, in the municipality of Peschiera del Garda. Since the lake impoundment in 1951, the outflow regime is measured some 500 m downstream the Salionze Dam, in the municipality of Monzambano.

### Land use analysis

The role of the land use/land class within the Garda catchment was investigated by comparing the results obtained by the application of the HILDA+ dataset with the CLC inventory, additionally assessing the effects of adopting a different number of land use classes. The HILDA+ model classifies the land use/cover states in 7 general categories (namely "urban", "cropland", "pasture", "forest", "grass/shrubland", "other land" and "water"). Instead, the CLC inventory provides a 44-classes land cover maps with spatial resolution of 100 m  $\times$  100 m since 1990, and every 6 years starting from 2000. Since the HILDA+ and CLC databases are updated to 2018 and 2019 respectively, we assumed no further variation over the remaining years to cover the entire time period of our analysis (1928-2020). The HILDA+ categories were extended starting from the original categories of the HILDA project (Fuchs *et al.*, 2013), which are designed according to the Intergovernmental Panel on Climate Change (IPCC) categories. The IPCC classification is consistent with the CLC inventory, thus allowing a proper comparison in this study. Interested readers are referred to Fuchs *et al.* (2013, 2015) and the related supplementary material for the harmonization procedure.

The monthly  $K_c$  values (Tab. 4) were first associated to the CLC dataset as reported in Provincia Autonoma di Trento (2006) and then grouped in the 7 classes of the HILDA+ dataset.

### Kriging methods for spatial interpolation

Kriging is a geostatistical technique that aims to make optimal, unbiased estimates of regionalized variables at unsampled locations using the structural properties of the so called semivariogram function and the initial set of data values.

The spatial autocorrelation structure of the scattered data is described by the semivariogram function  $\gamma(h)$ , which according to the Matheron algorithm (Matheron, 1963) is as follows:

$$\gamma(h) = \frac{1}{2N(h)} \sum_{i=1}^N (h) [Z(x_i) - Z(x_i + h)]^2, \quad (\text{S.28})$$

where  $N(h)$  is a function of the number  $n$  of sites considered and is referred to the number of pairs separated by the vector  $h$ ; the values of the variable of interest in the positions investigated are given by  $Z(x_i)$  and  $Z(x_i + h)$ . The dependency of eq. (S.28) on the lag distance  $h$  reveals that the semivariance tends to increase as the distance between measured points increase.

The chosen theoretical semivariogram, i.e., the best fitting model, is then adopted to estimate the values of the targeted variables in the unsampled locations via least-squares linear regression algorithms, i.e., the kriging methods. More details are available in Goovaerts (1997).

The kriging estimator is a function of the data with weights that follow from the unbiasedness constraint (i.e., zero mean estimation error) and the minimum square error condition. This implies that the error variance

$$\sigma_E(u) = \text{Var}\{Z^*(u) - Z(u)\} \quad (\text{S.29})$$

is minimized under the constraint that

$$E\{Z^*(u) - Z(u)\} = 0 \quad (\text{S.30})$$

where the random function  $Z(u)$  is described as the sum of a residual component  $R(u)$  and a trend component  $m(u)$ .

In this work, two different kriging methods were compared, the Ordinary Kriging (OK) and the Kriging with the External Drift (KED). The most adequate method was chosen throughout the Leave-One-Out Cross Validation (LOOCV) procedure. The difference between the methods described is due to the model considered for the trend  $m(u)$  of the random function  $Z(u)$ .

In the Ordinary Kriging (OK), local fluctuations of the mean are considered by limiting the domain of stationarity of the mean to the local neighbourhood  $W(u)$ , centered on the location  $u$  being estimated:

$$m(u) = \text{constant, but unknown, } \forall u' \in W(u) \quad (\text{S.31})$$

Hence, OK is an optimal predictor if the mean is assumed constant but unknown over the entire region of interest.

In some kind of processes, direct measurements of the variable of interest may be related to other categorical or continuous attributes and therefore can be supplemented with them. Instead of being modeled as a function of the spatial coordinates, in the Kriging with External Drift (KED) the trend  $m(u)$  is modeled as a linear function of a smoothly varying secondary (external) variable  $y(u)$ :

$$m(u) = a_0(u) + a_1(u)y(u) \quad (S.32)$$

where  $a_0(u)$  and  $a_1(u)$  are the constant but unknown trend coefficients within the search neighbourhood  $W$ ), implicitly estimated through the kriging system.

The Leave-One-Out Cross Validation (LOOCV) procedure predicts the value at an observational location by leaving out the observed value, using the other points to make the prediction. The procedure is then repeated for all the measurement points. To estimate the goodness of fit for the LOOCVs performed, the absolute value of the residuals, the variance of the error and correlations between observed and residuals, observed and predicted values, residual and predicted values were calculated.

## References

- Allen RG, Pereira LS, Raes D, Smith M, 1998. Crop evapotranspiration-guidelines for computing crop water requirements - FAO irrigation and drainage paper 56. FAO, Rome. Available from: <https://www.fao.org/3/X0490E/x0490e00.htm>
- Dalton J, 1802. Experimental essays on the constitution of mixed gases: on the force of steam or vapor from water or other liquids in different temperatures, both in a Torricelli vacuum and in air; on evaporation; and on expansion of gases by heat. Mem Lit Philos Soc Manchester 5:536-602.
- Fink G, Schmid M, Wahl B, Wolf T, Wüest A, 2014. Heat flux modifications related to climate-induced warming of large European lakes. Water Resour Res 50:2072-2085.
- Fuchs R, Herold M, Verburg PH, Clevers JG, 2013. A high-resolution and harmonized model approach for reconstructing and analyzing historic land changes in Europe. Biogeosciences 10:1543-1559.
- Fuchs R, Herold M, Verburg PH, Clevers JG, Eberle J, 2015. Gross changes in reconstructions of historic land cover/use for Europe between 1900 and 2010. Global Change Biol 21:299-313.
- Goovaerts P, 1997. Geostatistics for natural resources evaluation. Oxford, Oxford University Press: 483 pp.
- Hamon RW, Weiss LL, Wilson WT, 1954. Insolation as an empirical function of daily sunshine duration. Mon Weather Rev 82:141-146.
- Hargreaves GH, Samani ZA, 1985. Reference crop evapotranspiration from temperature. Appl Eng Agric 1:96-99.
- Jensen ME, Haise HR, 1963. Estimating evapotranspiration from solar radiation. J Irrig Drain Div 89:15-41.
- Majidi M, Alizadeh A, Farid A, Vazifedoust M, 2015. Estimating evaporation from lakes and reservoirs under limited data condition in a semi-arid region. Water Resour Manage 29:3711-3733.
- Martin JL, McCutcheon SC, Schottman RW, 2018. Hydrodynamics and transport for water quality modeling. Boca Raton, CRC Press: 816 pp.
- Matta E, Amadori M, Free G, Giardino C, Bresciani M, 2022. A satellite-based tool for mapping evaporation in inland water bodies: Formulation, application, and operational aspects. Remote Sens 14:2636.
- Mallucci S, Majone B, Bellin A, 2019. Detection and attribution of hydrological changes in a large alpine river basin. J Hydrol 575:1214-1229.
- Matheron G, 1963. Principles of geostatistics. Econ Geol 58:1246-1266.
- McMahon T, Peel M, Lowe L, Srikanthan R, McVicar T, 2013. Estimating actual, potential, reference crop and pan evaporation using standard meteorological data: a pragmatic synthesis. Hydrol Earth Syst Sci 17:1331-1363.
- Penman HL, 1948. Natural evaporation from open water, bare soil and grass. Proc R Soc Lond A Math Phys Sci 193:120-145.

- Piccolroaz S, 2016. Prediction of lake surface temperature using the air2water model: guidelines, challenges, and future perspectives. *Adv Oceanogr Limnol* 7:5791.
- Piccolroaz S, Healey N, Lenters J, Schladow S, Hook S, Sahoo G, Toffolon M, 2018. On the predictability of lake surface temperature using air temperature in a changing climate: A case study for Lake Tahoe (USA). *Limnol Oceanogr* 63:243-261.
- Piccolroaz S, Woolway RI, Merchant CJ, 2020. Global reconstruction of twentieth-century lake surface water temperature reveals different warming trends depending on the climatic zone. *Clim Change* 160:427-442.
- Priestley CHB, Taylor RJ, 1972. On the assessment of surface heat flux and evaporation using large-scale parameters. *Mon Weather Rev* 100: 81–92.
- Provincia Autonoma di Trento, 2006. [Piano Generale di Utilizzazione delle Acque Pubbliche]. [in Italian]. Available from: <http://pguap.provincia.tn.it/>
- Ravazzani G, Corbari C, Morella S, Gianoli P, Mancini M, 2012. Modified Hargreaves-Samani equation for the assessment of reference evapotranspiration in Alpine river basins. *J Irrig Drain Eng* 138:592-599.
- Toffolon N, Piccolroaz S, Majone B, Soja AM, Peeters F, Schmid M, Wüest A, 2014. Prediction of surface temperature in lakes with different morphology using air temperature. *Limnol Oceanogr* 59:2182-2202.
- Valiantzas JD, 2006. Simplified versions for the Penman evaporation equation using routine weather data. *J Hydrol* 331:690-702.

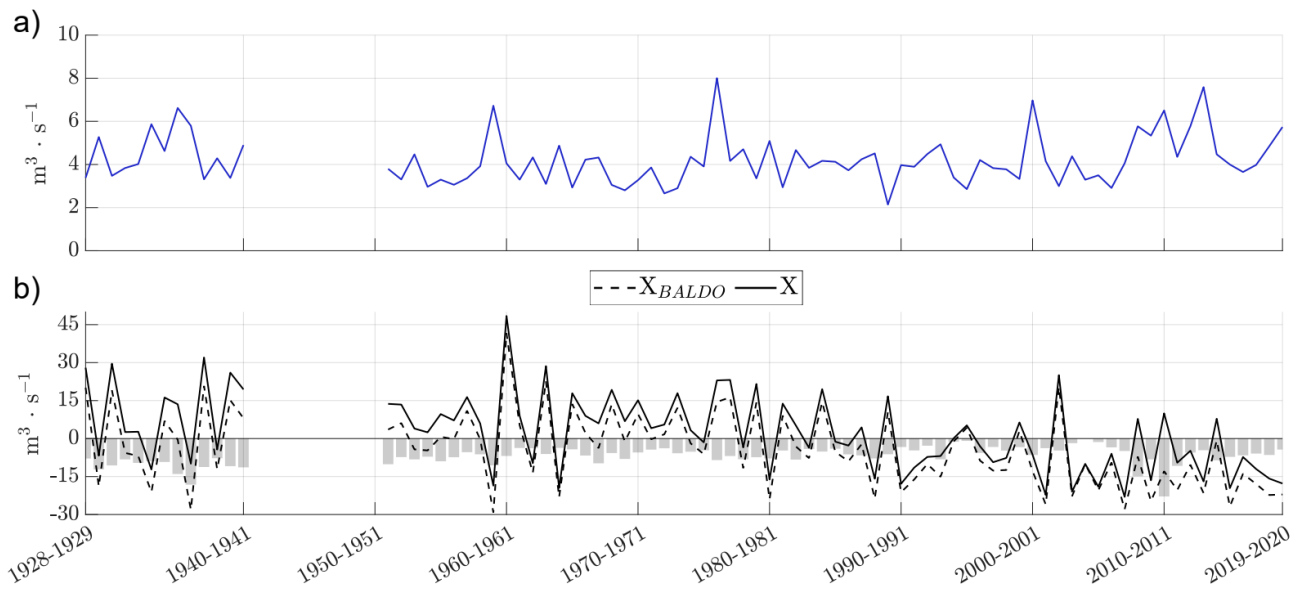


Fig. S1. a) The Mount Baldo catchment contribution evaluated as annual net precipitation. b) Residual term ( $X$ ) obtained by including (dashed line) or excluding (solid line) the Mount Baldo catchment in the annual water balance of Lake Garda. The grey bars indicate the difference between the two estimates.

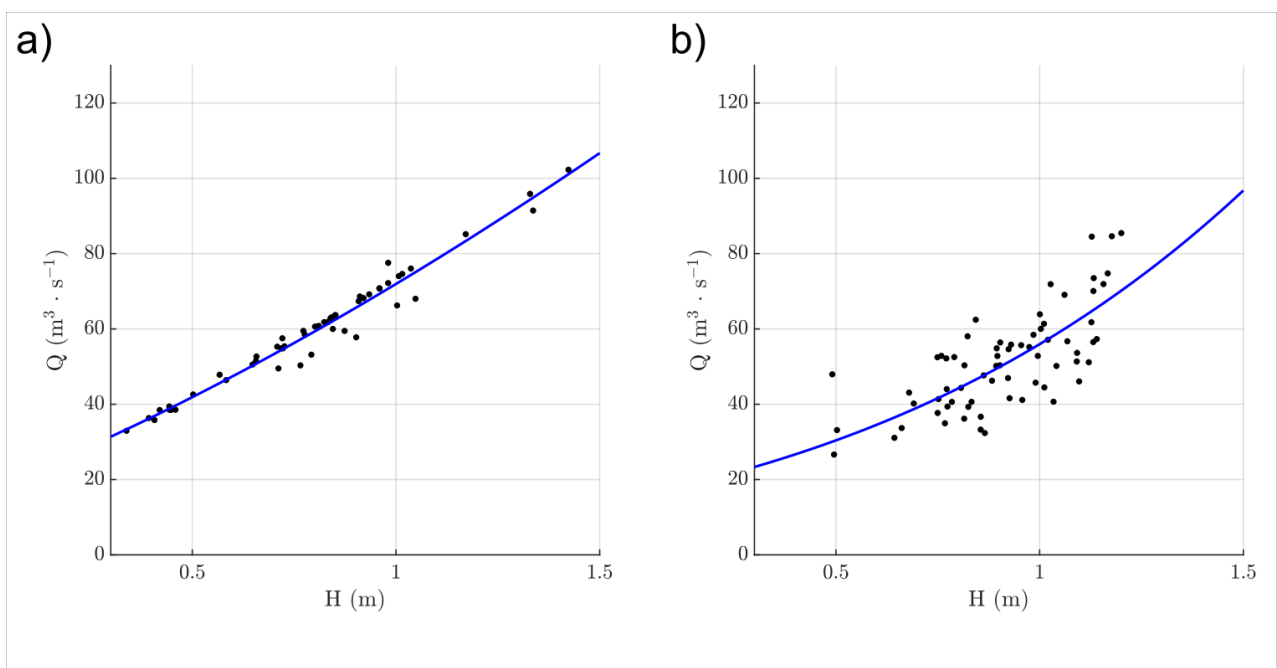


Fig. S2. Power-law curves found for Lake Garda between the lake water level and the outflow for the periods before (a) and after lake regulation (b). The values are averaged over the hydrological year.

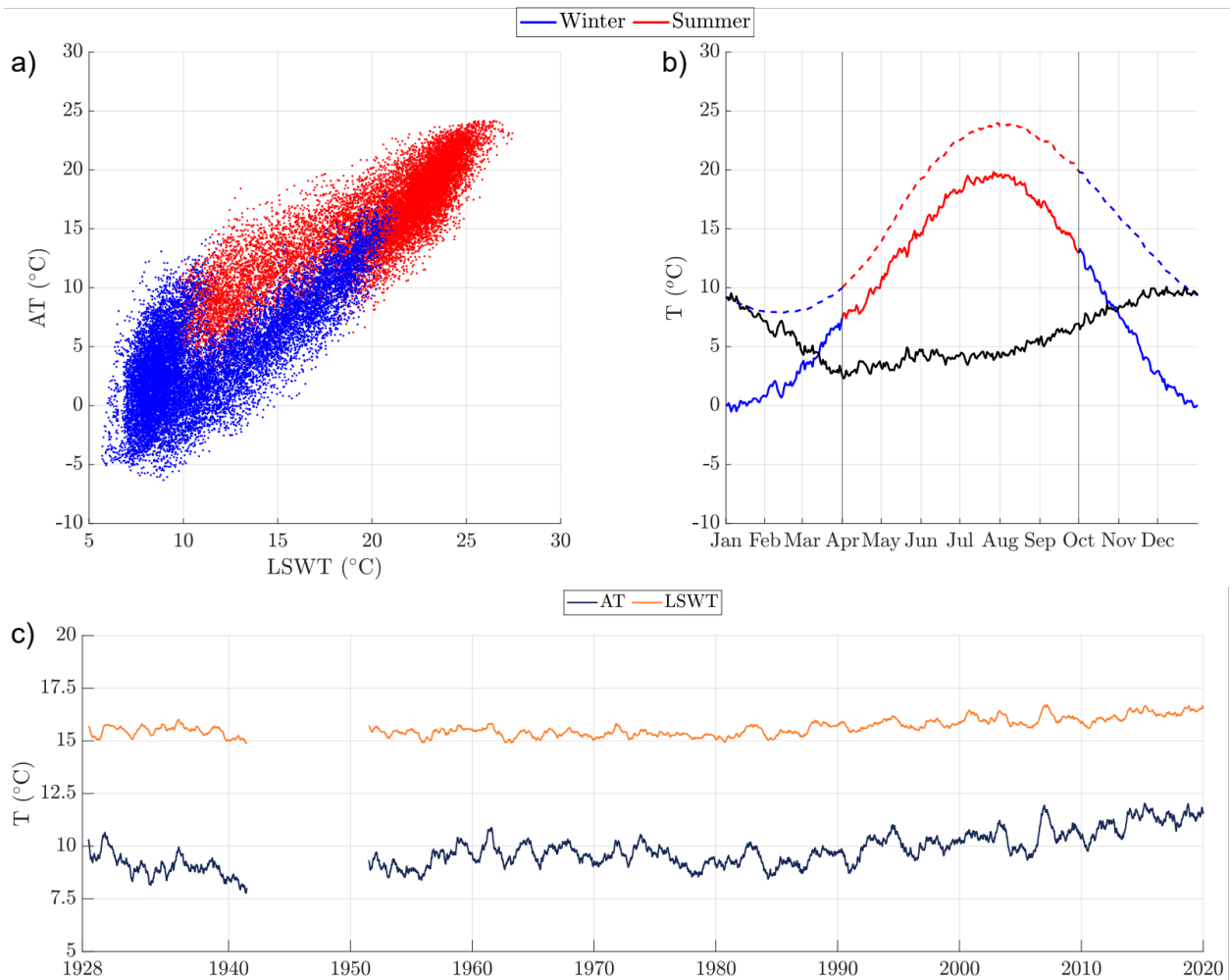


Fig. S3. a) Hysteresis cycle (daily values) of the air temperature (AT) and lake surface water temperature (LSWT) estimated for Lake Garda. b) Annual climatological cycles of air and water temperature (solid and dashed lines, respectively) and their difference (black solid line) for the whole period 1928-2020. Red and blue colours indicate values for the summer (April-September) and winter (October-March) seasons. c) Long-term time series (filtered with a 365-days moving average) of air temperature (dark blue) and LSWT (orange).

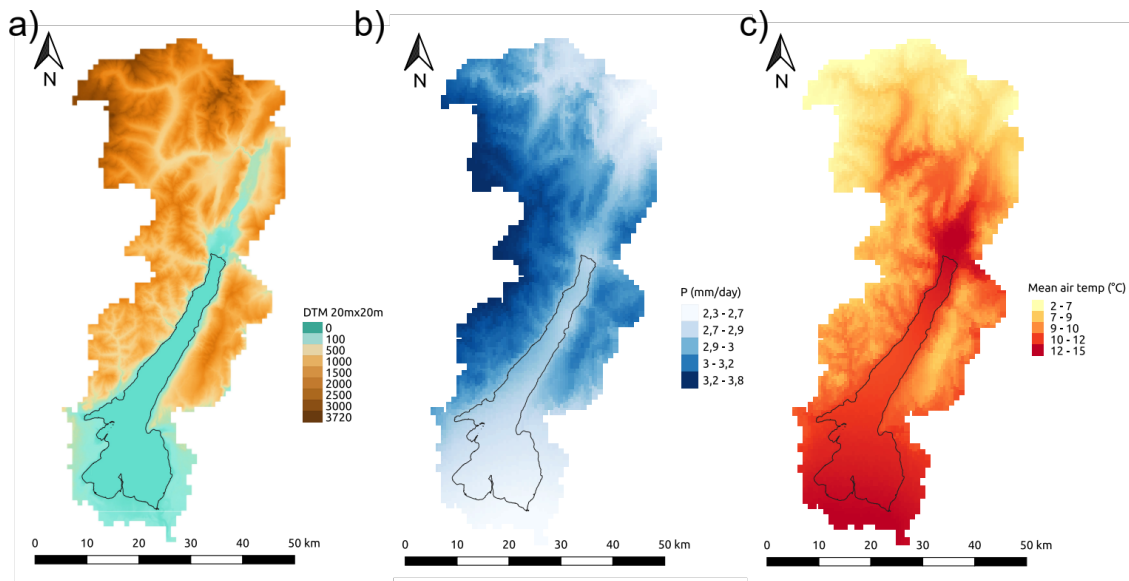


Fig. S4. a) Digital Terrain Model of the Garda catchment. b,c) Spatialized maps of the average values of precipitation and mean air temperature obtained from the kriging interpolation.

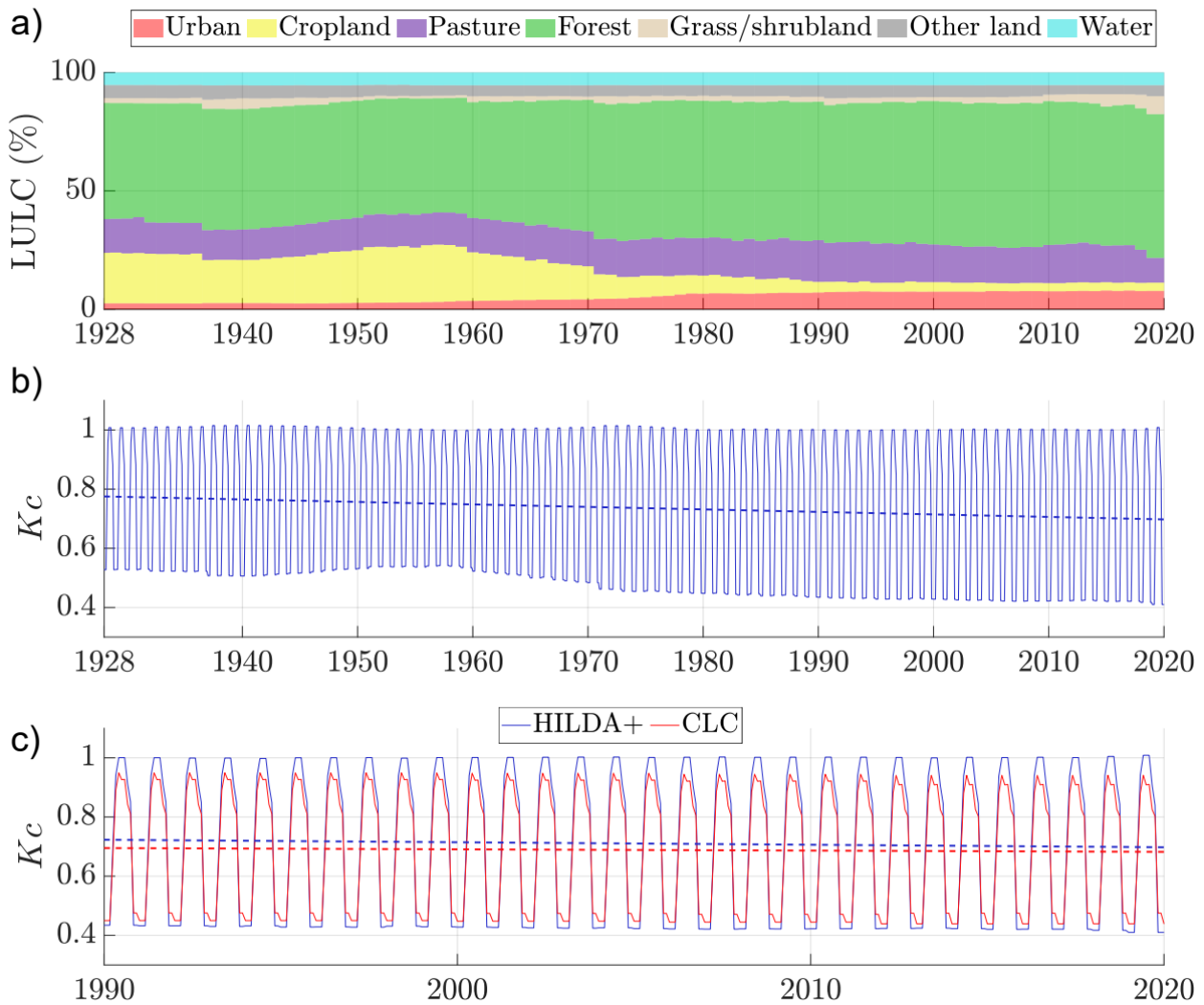


Fig. S5. a) Annual percentage of the HILDA+ land use land cover (LULC) categories within the Lake Garda catchment. b) Monthly average crop coefficient ( $K_c$ ) of the study area obtained starting from the HILDA+ dataset. c) Comparison between the annual average  $K_c$  obtained from the HILDA+ and Corine (CLC) datasets.